



PCCP

Influence of Early Stages of Triglyceride Pyrolysis on the Formation of PAHs as Coke Precursors

Journal:	<i>Physical Chemistry Chemical Physics</i>
Manuscript ID	CP-ART-04-2019-002025.R2
Article Type:	Paper
Date Submitted by the Author:	23-Aug-2019
Complete List of Authors:	Kozliak, Evguenii; University of North Dakota, Chemistry Sulkes, Mark; Tulane University, Chemistry Alhroub, Ibrahim; Tulane University, Chemistry Kubatova, Alena; University of North Dakota, Department of Chemistry Andrianova, Anastasia ; University of North Dakota, Chemistry Seames, Wayne; University of North Dakota, Chemical Engineering

SCHOLARONE™
Manuscripts

Influence of Early Stages of Triglyceride Pyrolysis on the Formation of PAHs as Coke Precursors

Evguenii Kozliak,^{a,*} Mark Sulkes,^{b,*} Ibrahim Alhroub,^b Alena Kubátová,^a Anastasia Andrianova,^a Wayne Seames^c

^a University of North Dakota, Department of Chemistry

^b Tulane University, Department of Chemistry

^c University of North Dakota, Department of Chemical Engineering

Address correspondence to evguenii.kozliak@und.edu [Evguenii Kozliak], cm06acf@tulane.edu [Mark Sulkes]

Abstract

Molecular beam (MB) time-of-flight mass spectrometry has been used to investigate thermal decomposition of triolein, to reveal the mechanisms of low temperature soot/coke formation characteristic for triglycerides (TGs). Mass detected pyrolysis products were observed at incremented temperatures using both VUV single photon ionization (general product detection) and REMPI based selective detection of aromatic products. To augment the simple mass characterizations, we have employed stoichiometric considerations; we have supplemented the analysis further by using the detailed information available from product analysis of batch reactor TG cracking. Both the VUV photoionization and batch reactor studies indicated that formation of C₇-sized stable products is a marker of significant triolein decomposition that is coupled with PAH formation. A significant fraction of the C₇ species observed likely formed as a result of a C-C bond scission at the allylic position to the ω-9 double bond of oleic acid. REMPI detection indicated a high specificity for PAH formation at three distinct molecular weight values, 276, 352 and 444 amu (the latter being a fullerene precursor). The stoichiometric analysis has shown that these PAHs likely arise from condensation reactions of either C₇- or C₈-sized fragments (three, four and five, respectively). The C₈-sized intermediate would become essential whenever the PAH product of C₇ fragment condensation contained an odd number of carbon atoms, resulting in a less stable aromatic structure with an incomplete double bond conjugation. MB experiments involving either addition or *in situ* generation of hydrogen resulted in an enhancement of lower molecular weight PAH formation, *i.e.*, a decrease in the effective number of condensing fragments. In contrast, an increase in temperature yielded the opposite effect.

1. Introduction

Triglycerides (TGs) are abundant plant products (*e.g.*, crop oils) that potentially can provide sustainable hydrocarbon fuel production via thermal or catalytic cracking. For this reason, TG pyrolysis chemistry has been studied for many years, primarily through batch reactor studies. A number of key chemical reactions have been identified by this approach,¹⁻⁸ though a comprehensive understanding is far from complete. Hindrances include the necessity of time-consuming heating of reaction vessels to high temperatures and the rather long reaction times required before product sampling; real time monitoring of reaction chemistry is impractical. While batch reactor studies can provide a thorough and quantitative identification of *volatile* terminal products,^{9,10} higher mass products, particularly PAHs with more than six fused rings, are not amenable to gas chromatography (GC) analysis, the main analytical method in this area. A further inhibition of analysis arises because large PAHs are embedded into the solid phase products (coke).

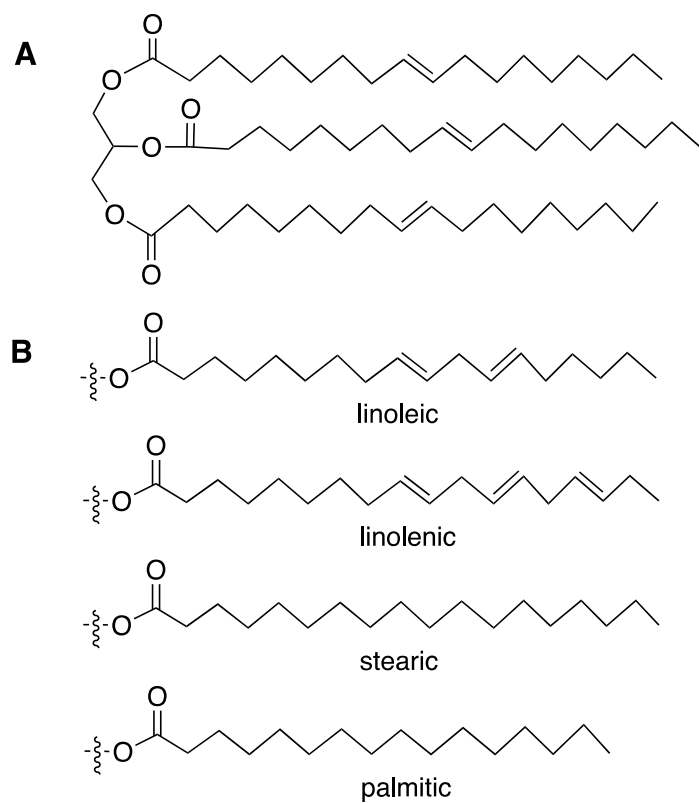
Our previous work demonstrated that standard mass spectrometric molecular beam methods (MB-TOFMS) can offer a fruitful alternative approach for studying TG pyrolysis.^{11,12} Overall product chemistry can be monitored with 118 nm single photon (10.5 eV) VUV ionization (SPI); aromatic specific product detection can be done quickly with a simple REMPI approach, two photon ionization at 266 nm. As a result, product chemistry as a function of temperature can be followed in real time using both methods. The REMPI measurements have for the first time revealed an unusual PAH chemistry in TG pyrolysis. PAH formation was unexpectedly selective and began at surprisingly low temperatures, <300 °C.¹² We found that PAHs of certain molecular weight (MW) and size were preferentially formed, particularly those corresponding to detected photoions at m/z 276, 352 and 444. (Henceforth, we will designate TOFMS peak values obtained for ions in m/z units; we will apply amu units only to neutral species from which photoions were produced.)

The observed PAH formation chemistry^{11,12} has transformed our perspective on these system studies. While better understanding the chemistry of TG pyrolysis may contribute to renewable fuel production, TG pyrolysis, employing MB-based real time analysis of gas phase products, now presents itself as a novel and experimentally tractable system for studying nascent soot precursors: selective PAH production in this system ensues at temperatures far lower than in combustion.

In spite of its significant advantages, the MB-TOFMS approach has weaknesses. Besides limitations in product quantification, the major weakness is limited ability to make product identifications, only on the basis of mass. For low mass non-aromatic species ($m/z < \sim 100$) this deficiency can be mitigated by use of simple stoichiometric based attributions (*e.g.*, Table 1 in this paper). For high mass aromatic species we also can make some plausible formula arguments and possible assignment of base species in some observed homology series.¹²

Additional direct experimental data obviously would be highly useful. One powerful experimental approach that has yielded great insight in model combustion reactions is the mass dependent measurement of photoionization efficiency (PIE) as a function of VUV single photon energy, a capability available at synchrotron facilities. For example, Zhao et al.¹³ recently used measured PIE curves to make isomeric characterizations of $C_{13}H_{10}$ ($m/z = 166$ for major isotopic peak) products that were formed in a reaction under combustion-like temperatures, reacting 2-naphthyl isomer ($C_{10}H_7$) with allene (C_3H_4) and methylacetylene (C_3H_4). For comparison with reference data, Zhao et al. needed to measure PIE calibration curves for six distinct $C_{13}H_{10}$ isomers. Unfortunately, an analogous approach would be almost insurmountably difficult for the key PAHs observed in our studies: The NIST PAH structure index¹⁴ lists 15 PAH structures for MW 276 and 48 for MW 352. There are no tabulations for MW 444, where there would be a very large number of possible isomers. Similarly, IR/UV ion dip spectroscopy, unavailable to us, would be invaluable in providing mass selected species information.¹⁵

For complementary data that might yield further insight into the MB-TOFMS results, we have turned to batch reactor experiments;¹² we make similar recourse to analogous complementary data in this paper. Detailed analyses of prior batch reactor TG thermal cracking experiments have revealed a relatively selective pattern of product molecular sizes. For example, when canola oil, a plant oil rich in oleic acid, was thermally cracked, GC-MS/FID product analysis revealed a homology profile of carboxylic acids featuring three peaks, at C_2 - C_3 , C_7 and C_9 - C_{10} molecular sizes.¹⁻³ Oleic acid contains a ω -9 double bond (Scheme 1), which is believed to facilitate decomposition into these fragments. This observation led to a plausible explanation of mechanistic pathways of TG pyrolytic product formation.² The homology patterns of non-oxygenated products, monocyclic hydrocarbons and alkenes, showed a single, though broad, peak centered near the C_7 size.³



Scheme 1. Triglycerides used in this study. A. Triolein B. Other carboxylic acid moieties replacing some oleic acid moieties in canola oil.

Our MB-TOFMS observations in this paper are therefore combined with comparable batch reactor results obtained from the pyrolysis of canola oil, containing a high proportion of oleic acid; this naturally occurring feedstock was used instead of triolein in relatively large scale experiments due to the much higher price of triolein. The chemical structures of triolein and main carboxylic acid moieties of canola oil are shown in Scheme 1. The batch reactor results herein, not reported earlier, lead to detailed homology profiles of alkanes, all hydrocarbons and total products. While keeping in mind the difference in process timescales, we attempt to correlate the MB-TOFMS results with the batch reactor product homology profiles.

A significant portion of batch reactor TG pyrolysis products (10-20%) comprised a solid coke/tar fraction,³⁻⁸ largely representing soot and its precursors. While soot formation has been investigated extensively for higher temperature processes such as combustion,^{16,17} TG thermal cracking occurs at significantly lower temperatures, 300-450 °C. For TG pyrolysis processes, a better understanding of coke/tar formation is of particular interest. On the one hand, these products are undesirable in pyrolytic processes to create transportation fuels and in food chemistry. On the other hand, they are potentially valuable as a feedstock to produce high purity coke (including fullerenes and their precursors), carbon black, or carbon fibers.

In connecting the MB results to those obtained by the GC analysis of TG thermal cracking products, we concluded in our previous work that the observed PAHs were formed as a result of associative chemical reactions between hydrocarbon fragments of several predominant sizes, C₇-C₁₁.¹² However, direct comparison between the coke precursors and liquid products of TG pyrolysis by using GC is hindered, because the former appear to segregate from the latter very early in the process.¹² This assumption was recently confirmed by Fanglin et al., who showed that high MW PAHs can be recovered from TG pyrolytic products only by a solvent extraction of the coke formed.¹⁸

A major initiative in this paper is to assess the effects of added H₂ on PAH product formation. Batch reactor experiments had indicated that the presence of externally added H₂ did not positively impact PAH formation at temperatures above 400 °C but did show effectiveness at lower temperatures.¹ The addition of hydrogen is known to initiate and/or speed up decarboxylation of triglycerides and carboxylic acids.¹⁹⁻²¹ A concomitant bonus in the completed H₂ study, reported herein, has been further insight into the likely *in situ* chemistry that sensitively depends on sample medium and sample holder geometry/dimensions.

Another key initiative of this paper, comparing concurrent VUV SPI and REMPI mass spectra, is to establish detailed connections between non-aromatic products of low MW ($< \sim 100$ amu) and the appearance of selectively formed PAHs of rather high mass (276, 352, 444 amu). As already noted, analogous real time studies are not possible in batch reactor experiments. Possibilities for bulk product studies by direct MS, instead of GC, are similarly limited. Such studies are usually conducted in the liquid phase, where the solvent or products present in large amounts may overwhelm the detector. To the best of our knowledge, no direct MS analysis results have been reported for TG pyrolysis, perhaps due to this constraint.

It is the combination of the approaches employed herein that have allowed us to pinpoint the most important size PAH building blocks as C_7 fragments; stoichiometry then determines why and when one C_8 fragment has to replace one of the C_7 fragments to yield fully conjugated PAHs.

2. Experimental

2.1 MB-TOFMS experiments

Details of the MB-TOFMS experiments have been described elsewhere.^{11,12} A two stage sample holder was employed, since efforts to use single stage configurations produced poorer results. A dimensioned schematic is shown in Figure 1; the TOFMS part of the setup has been described in previous publications.^{11,12} The stages were solidly packed with deactivated glass wool. One drop of liquid triolein (~ 16 mg, Sigma-Aldrich, $>99\%$ purity) was deposited in the upper portion of the first stage, after which further glass wool was added. A second stage ending in a $d \approx 100 \mu\text{m}$ pinhole, also packed with deactivated glass wool, was attached to the first via a 1/8 NPT coupling. The C/C' results shown in Figures 2 and 3 were obtained using a first stage of similar dimensions to the one used in the A/A' and B/B' experiments but with a denser glass wool network.

As the temperatures were raised, continuous gas expansions were carried out with carrier gas backing

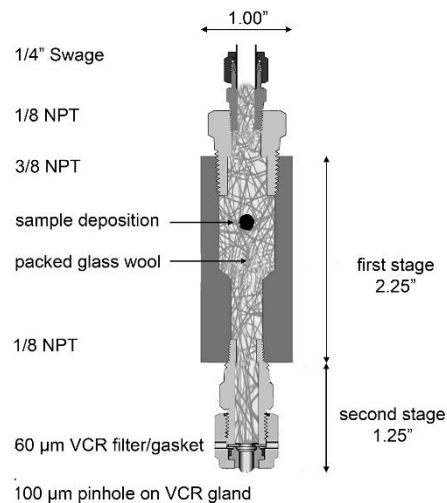


Figure 1. Schematic of sample holder. The main body of the first stage was custom machined from brass. Other fittings were standard Swagelok components, all in stainless steel.

pressures of ~ 0.5 atm absolute. The center stream of the gas expansions was skimmed. Nd:YAG laser pulses effected soft photoionization (*i.e.*, little or no parent ion fragmentation), either at 118 nm (frequency tripling of 355 nm pulses in rare gas) or at 266 nm (Nd:YAG 4th harmonic). The 118 nm (10.5 eV photon energy) pulses produced single photon ionization of almost all neutral species present and the ion yields roughly reflected relative species concentrations. With aromatic species, 266 nm pulses can produce nearly resonant two photon ionization. Using unfocused pulses of ~ 1 mJ, robust ion signals were observed for aromatics. In contrast, for non-aromatic neutrals the process would be non-resonant two photon ionization. Under the same conditions, these ion signals were undetectably small. Following photoionization, cationic species underwent TOFMS in a reflectron-based TOF configuration. TOF mass waveforms were acquired with both 118 nm PI and 266 nm PI at incremented sample temperature intervals.

In all experiments using 118 nm PI, we always performed the following procedure at one or more temperatures, to assess effects of residual 355 nm radiation. First, product detection was done with 118 nm PI (rare gas in the tripling cell); the detector voltage was set so that the largest product peaks were $\sim 80\%$ of the detection dynamic range. After TOFMS were acquired, rare gas was removed from the tripling cell, so that 355 nm radiation alone was present; additional TOFMS were acquired with the same detector voltage and the results compared.

Experiments proceeded by acquiring TOFMS at successively higher sample temperatures. We also carried out analogous He flow sample heating sequences for the purpose of collecting the products that emerged from the pinhole. In these instances, a liquid nitrogen-cooled copper cold finger holding a 10 mL beaker was placed just above the skimmer, such that products exiting the pinhole were collected in the beaker. For the product collections, carrier gas flow conditions replicated those in TOFMS experiments; the stepped heating duration intervals also matched TOFMS experiments, terminating at ~ 400 °C. After each cumulative collection was completed, the collection beaker was brought to room temperature, sealed with Parafilm, then stored in a freezer until further analysis was completed.

2.1.1 APCI characterization of cumulatively collected products

Analysis of the collected products was performed via atmospheric pressure chemical ionization-high resolution time-of-flight mass spectrometry (APCI-HR TOFMS) using an

Agilent 6210 HR TOFMS (Agilent Technologies, Santa Clara, CA, USA). In this method, the gaseous solvent (methanol) and fully or partially cracked triolein sample were ionized by a highly charged corona discharge electrode. APCI allowed for soft ionization of nonpolar or slightly polar molecules by removing an electron from a neutral molecule, without depositing enough internal energy to cause fragmentation. Coronene standard (Sigma-Aldrich, (St. Louis, MO, USA), a mixture of sixteen PAHs (Sigma-Aldrich) and the TG trilinolenin standard [Nu-Chek Prep. Inc. (Elysian, MN, USA)] were used for APCI-HR TOFMS condition optimization. The most efficient ionization was achieved in the positive APCI mode with a corona current of 5 μA , capillary and fragmentor voltages of 4000 and 150 V, respectively. Ammonium acetate with a final concentration of 2.5 mM in 1:1 methanol/water (v/v) was used as a background electrolyte.

2.1.2 Post processing analysis of MB-TOFMS

As previously described,¹¹ we have employed multivariate curve resolution (MCR) and x loading plots of principal components to characterize and clarify evolving product chemistry trends. These methods have previously been applied to electron impact ionization MS of evolving woody biomass pyrolysis.²² MCR synthesized mass spectra can be correlated to early, intermediate, and high temperature regimes, clarifying trends observed in the direct experimental set of TOFMS. Similarly, examination of the x loadings of the principal components (*i.e.*, correlation coefficients of various mass peaks within a given PC), mainly for the major PC, PC-1, can be helpful in clarifying correlations in growth/diminution of product peaks compared to one another. For input in our computations using the multivariate analysis program The Unscrambler 10.3, we have re-expressed the experimental TOFMS waveforms as intensity variables in 1 m/z “boxes.” The computed 1 m/z mass resolution causes some, but not particularly severe, diminution of mass resolution compared to direct TOFMS waveforms.

2.1.3 Experimental approach and setup

Over numerous runs involving different TGs, we have observed sensitivity in the details of the product chemistry as a function of apparently small changes in the sample holder, sample

medium (deactivated glass wool in current experiments), and placement of TG into the medium. If comparisons are to be made between TOFMS employing pure He carrier gas versus He with added H₂, care must be taken that the sample handling and sample deposition conditions are the same. To achieve this aim, successive sample preparations using the same sample holder stages were first run with pure He carrier gas, with both 118 nm PI and 266 nm PI mass spectra recorded as a function of increased heating temperature. These “training spectra” were recorded with close observation of the preparation details until successive runs displayed no more than minor differences in mass spectra at the same temperatures. At this point, additional run sequences were carried out under the same conditions using carrier gas that was 10% H₂ in 90% He. Experimental TOFMS waveforms were recorded and averaged at 20-40 °C intervals.

Spectra with and without hydrogen addition are designated in Figs. 2-3 as A & B and A' & B' with 118 and 266 nm photoionization, respectively. If sample conditions are identical, observed A/B and A'/B' differences are due only to hydrogen addition. However, subtle sample handling changes can make for nontrivial product chemistry differences. To qualify and contrast the A/A' with B/B' differences, also possibly to obtain some insight into their cause, we present results with a slightly different stage 1/2 sample holder (results C/C' in Figs. 2-3). In this case, denser glass wool packing took place. As a result, *in situ* hydrogen generation appears to have been facilitated.

Comparisons in A/B could be made between product mass spectra at similar temperatures with and without added H₂. Key temperatures for comparison/examination are ~260-280 °C, where a variety of aromatic products begin to appear, and ~380-400 °C, where selectively formed PAHs have become predominant. (See supplemental Figure S2, showing TOFMS as a function of temperature for pure He carrier gas, 118 nm and 266 nm PI. The appearance of new product peaks at a given temperature, relative to baseline results, indicates the onset of pyrolysis products.) One approach was to compare TOFMS recorded at similar temperatures with and without added H₂. Another approach was to compute MCR components for each total set of TOFMS, with and without added H₂, sets of TOFMS ranging from low temperatures to highest temperatures.

In each instance, three computed MCR components resulted. One corresponded to a product mass spectrum at the lowest temperatures, the second to mid-range temperatures (~280 °C), and the third to the highest temperatures. The advantages of the MCR approach are that the

entire sets of TOFMS are condensed to a smaller number of comparison mass spectra, with peak growth trends magnified compared to any single TOFMS. While either type of comparison resulted in similar observations, because of the apparent advantages we display MCR components in Figures 2-3. Figure 4, considered later, shows the computed PC-1 x loadings for the B (118 nm PI) and B' (266 nm PI) series of TOFMS—pure He case; the actual TOFMS appear in Fig. S2.

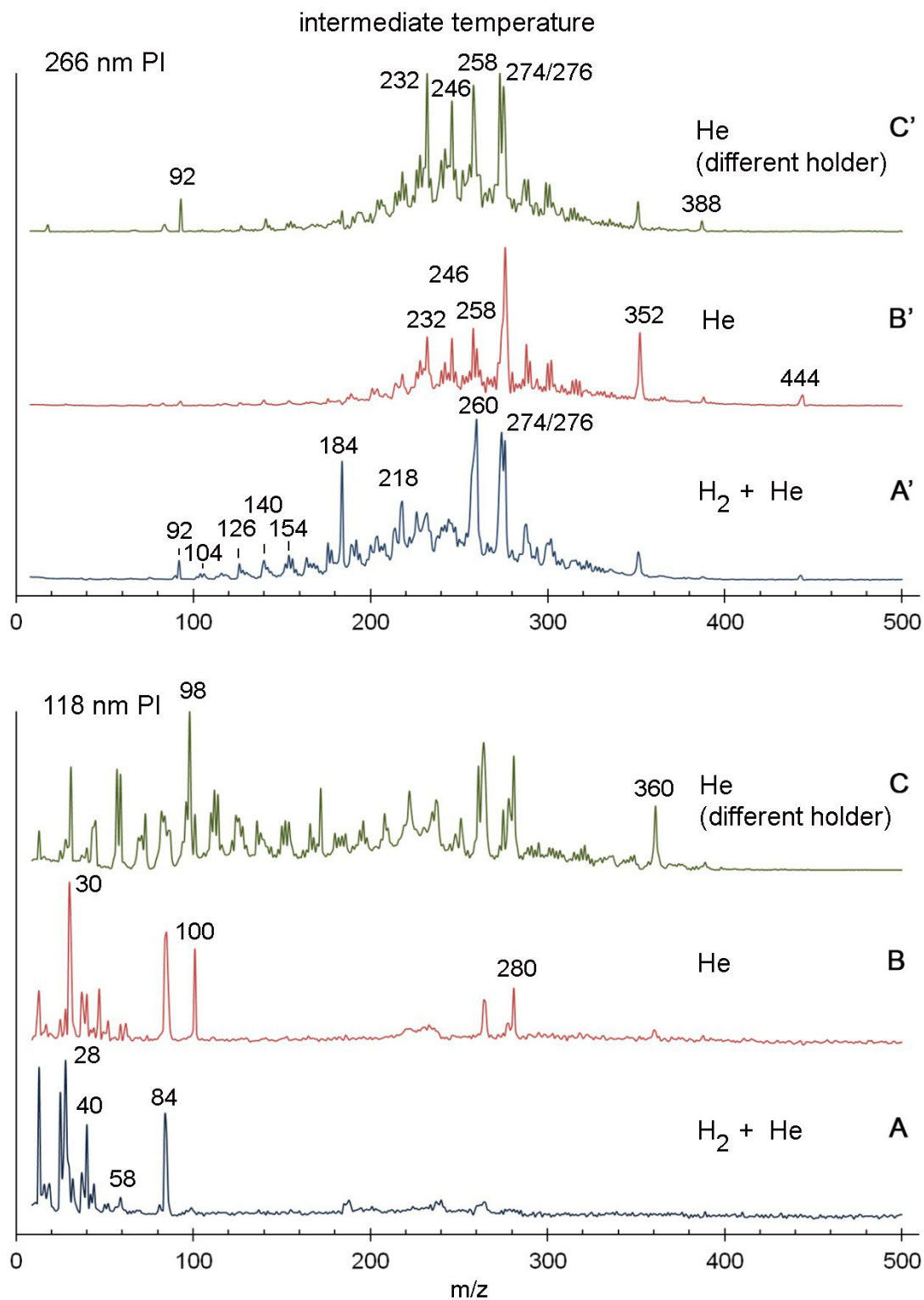


Figure 2. MCR components corresponding to intermediate (~ 280 °C) temperatures. Labels A, B and C (A', B, and C' for 266 nm photoionization specific for aromatics) reflect the difference in sample preparation conditions – 10% H₂ in the carrier gas, pure helium as a carrier gas, and additional glass wool in the sample holder to promote the atomic hydrogen formation, respectively. In these mass spectra and others in following figures, the labels within the mass spectra denote specific m/z values.

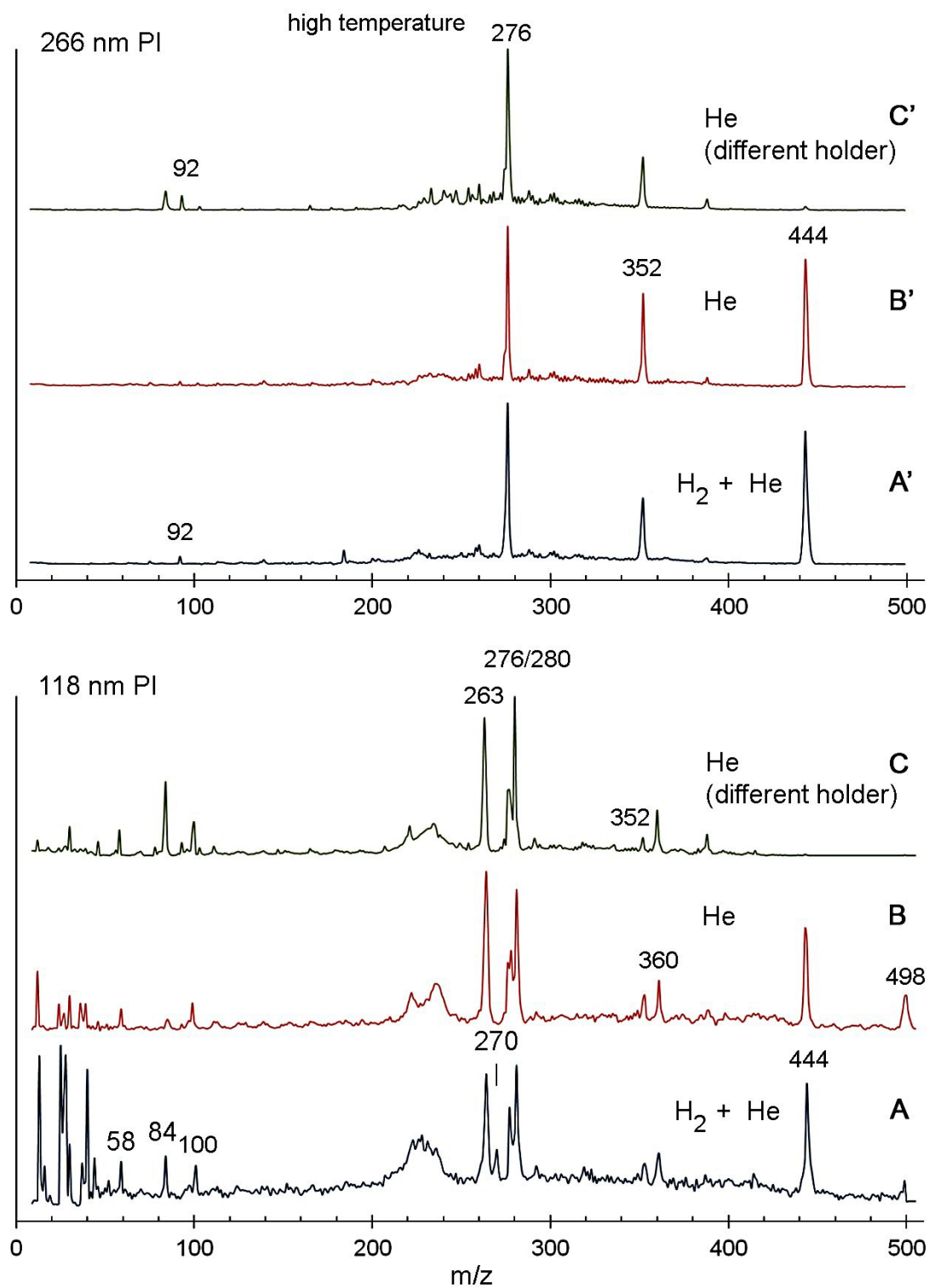


Figure 3. MCR components corresponding to high (~380 °C) temperature. Labels A, B and C (A', B, and C' for 266 nm photoionization specific for aromatics) reflect the difference in sample preparation conditions – 10% H₂ in the carrier gas, pure helium as a carrier gas, and additional glass wool in the sample holder to promote the atomic hydrogen formation, respectively.

2.1.4 Stoichiometric analysis for likely characterization of product peaks observed

The MB-TOFMS provide no structural information, only peak m/z values. However, we have previously shown that for PAH species, a simple stoichiometric analysis based on the combination of nearly-integer atomic masses of carbon, oxygen and hydrogen can accurately estimate the number of carbon atoms for a given molecular weight. As a result, some likely structural insight was possible for relatively low MW PAH molecules.¹²

We have now extended this method to non-aromatic low MW products of TG pyrolysis. Table 1 shows the hydrocarbon and carboxylic acid species pertinent to observed ions whose neutral species MW do not exceed 120 amu. Hydrocarbons, monocarboxylic acids, and dicarboxylic acids were observed in batch reactor studies as the major products of TG thermal cracking.^{1,3} The less expected species, alcohols and aldehydes/ketones, which were either not observed or recovered only in trace amounts among the batch reactor TG pyrolysis products, are listed in Table S1.

Table 1. Molecular weights of expected species for possible correlation with observed MB-TOF low MW (below 120 amu) peaks.

Species Types	C ₁	C ₂	C ₃	C ₄	C ₅	C ₆	C ₇	C ₈
Hydrocarbons*:								
Alkanes	16	30	44	58	72	86	100	114
C _n H _{2n+2}	CH ₄	C ₂ H ₆	C ₃ H ₈	C ₄ H ₁₀	C ₅ H ₁₂	C ₆ H ₁₄	C ₇ H ₁₆	C ₈ H ₁₈
Alkenes & cycloalkanes		28	42	56	70	84	98	112
C _n H _{2n}		C ₂ H ₄	C ₃ H ₆	C ₄ H ₈	C ₅ H ₁₀	C ₆ H ₁₂	C ₇ H ₁₄	C ₈ H ₁₆
Alkynes, cycloalkanes, alkadienes		26	40	54	68	82	96	110
C _n H _{2n-2}	-	C ₂ H ₂	C ₃ H ₄	C ₄ H ₆	C ₅ H ₈	C ₆ H ₁₀	C ₇ H ₁₂	C ₈ H ₁₄
Aromatic, with saturated side chain		-	-	-	-	78	92	106
C _n H _{2n-6}						C ₆ H ₆	C ₇ H ₈	C ₈ H ₁₀
Aromatic, with unsaturated side chain		-	-	-	-	-	-	104
C _n H _{2n-8}								C ₈ H ₈
Carboxylic acids:								
Monocarboxylic acids	46	60	74	88	102	116		
C _n H _{2n} O ₂	CH ₂ O ₂	C ₂ H ₄ O ₂	C ₃ H ₆ O ₂	C ₄ H ₈ O ₂	C ₅ H ₁₀ O ₂	C ₆ H ₁₂ O ₂		
Dicarboxylic acids	-	90	104	120				
C _n H _{2n-2} O ₄		C ₂ H ₂ O ₄	C ₃ H ₄ O ₄	C ₄ H ₆ O ₄				

* The corresponding free radicals, potential intermediates, have the MW less by 1 amu.

Species listed in the tables form homology series, *i.e.*, are 14 amu apart, upon the addition of an extra carbon atom. The correctness/consistency of assignments for species in the TOFMS can be verified by observed 14 m/z differences between the nearest homologs.

2.2 Canola oil pyrolysis experiments

The reactions were carried out in a 1-L laboratory scale reactor made of stainless steel. The reactor was rated for a pressure of up to 37.2 MPa (5400 psia), compatible with hot-charge reactants injection and the removal of reaction-temperature volatile materials at reaction pressure. The reactor, fitted with a stirrer, was externally heated by electrical ceramic heaters. All connections were made with 1/8" or 1/4" stainless steel tubing (Swagelok).

Pyrolytic experiments were carried out at 430 °C under vacuum. A Hydra Data Logger was used to monitor the reactor pressure and temperature once every 6 seconds. After the set temperature was reached (in ca. 30 min), the reaction mixture was maintained at this temperature for 60 min.

The experiments were conducted in triplicate. At the end of each experiment, the reaction products (present mostly as vapors at reaction pressure and temperature) were transferred from the reaction mixture by slow opening of the high-pressure vent valve. This gaseous reaction mixture was passed through a water-cooled condenser where the organic liquid product (OLP) was condensed using water at 25 °C. Following the separation of the gas and solid (coke/tar) phases, the OLP was collected in pre-weighed flash traps. The OLP was characterized by its chemical composition as described in the following section.

2.2.1 OLP chemical characterization

The detailed chemical analysis was performed using an Agilent 7890 gas chromatograph equipped with mass spectrometric (Agilent 5975) and flame ionization detectors (GC-MS/FID), with an Agilent 7683 series autosampler. The separation was performed on a DB-Petro capillary column (100 m long, 0.25 mm id, with a 0.5 μm film thickness, J&W Scientific, Rancho Cordova, CA, USA) at a constant helium flow rate of 1.5 mL/min. Samples (0.2 μL) were injected with a split ratio of 1:30 into a programmed temperature vaporizer at 25 °C, which was heated at a rate of 720 °C/min to 350 °C. The GC temperature program started at 5 °C followed by a gradient of 2.5 °C/min up to 300 °C, with the final hold of 15 min. The FID and MS

temperatures were set at 350 °C and 280 °C, respectively. The MS data were acquired using electron ionization in a full scan of 50-500 m/z . Quantification was done using the internal standard method as described previously.¹⁰

Identification was performed by matching observed product retention times to those of known chemicals in standard mixtures and confirmed using the mass spectra. For chemicals whose standards were unavailable (long-chain substituted cycles, particularly, branched and polycyclic), the tentative identification was performed using the MS library. Details of identification and quantification for pyrolytic products are described by Stavova et al.¹⁰

3. Results and Discussion

3.1 Qualification of experiments to observe H₂ addition effects in MB-TOFMS

MCR mass spectra corresponding to intermediate temperatures (~280 °C) for triolein are shown in Figure 2, for 118 nm PI in the lower portion (unprimed letter labels) and 266 nm PI in the upper portion (primed letter labels). Fig. 3 similarly shows computed MCR mass spectra corresponding to high temperature (~380 °C). In both figures, the A/A' mass spectra are with 10% H₂ in He while B/B' employ the same sample holder and conditions with pure He. The cases for comparison are A versus B, A' versus B'. Similarly, C and C' are the spectra obtained with extra glass wool designed to enhance the atomic hydrogen generation (see **Materials and Methods**).

As Figs. 2 and 3 make clear, differences between the A to C and A' to C' mass spectra are particularly evident in the lower (~280 °C) temperature range but less evident in the higher (~380 °C) range. The overall observations are consistent with the batch reactor results, where added hydrogen did not significantly impact thermal cracking liquid hydrocarbon product formation at temperatures above 400 °C.¹ Both the MB and batch reactor trends can be explained by ample *in situ* hydrogen formation at higher temperatures, as a result of multiple dehydrogenation reactions. A more detailed discussion of the observed trends at ~280 °C and then ~380 °C follows.

3.2 Comparison of MB-TOFMS and MS-APCI results: Apparent high MW product fragmentation

The 118 nm PI-TOFMS taken at successively higher temperatures revealed the first appearance of non-aromatic pyrolytic products at ~ 220 °C. (See the detailed TOFMS data in Supplement, Fig. S2.) One might have expected the initial observation of some high mass species, arising directly from early fragmentations of the TG. However, only low mass species, $m/z < 100$, were observed. At temperatures approaching the intermediate regime, as shown in Fig. 2 (~ 280 °C), the beginning appearance of higher MW species (m/z 263, 276, 280, 360) is consistent with associative chemical reactions of smaller-size species rather than primary fragmentation. Such associative reactions (called henceforth “associative chemistry”) are slightly underway in Figs. 2 A/B and quite extensive in Fig. 2C. As with triolein, MB-TOFMS experiments using oleic acid also revealed only small fragments at lower temperatures. Higher MW species apparently were only formed later due to associative chemistry.¹¹

In contrast, batch reactor pyrolytic studies conducted with canola oil (rich in oleic acid) typically showed significant formation of linear alkanes and alkenes in the C_3 - C_{16} size range (Figure 5). While the 118 nm PI-TOFMS do not show any tri-, di- or monoglycerides or unfragmented oleic acid (282 m/z), we did detect some of these species in subsequent APCI-HR-TOFMS analysis of cumulatively collected products exiting the pinhole. Although the APCI analysis showed little or no intact triolein, numerous significant product peaks appeared between $m/z \sim 480$ -650 (see Suppl. Figure S1). The ionization potential of gas phase triolein is in the low 7 eV range.²³ Since photoionization should have occurred, these high MW species were not observed in the MB-TOFMS either because: (1) they were not present in appreciable concentrations after the pinhole or (2) following photoionization, initial ions underwent fragmentation to smaller ionic species. The APCI analysis appears to eliminate possibility (1), so evidently fragmentation of these ions occurred in MB-TOFMS.

In the 118 nm PI TOFMS (Fig. 2 A-C and Fig. S2), fragmentation of the expected high m/z non-aromatic ions could be due to effects from residual 355 nm photons. While we employed a setup that reduces the residual ~ 15 mJ of 355 nm present,¹² nontrivial residual amounts still can produce effects. Optimum conversion efficiency of 118 nm generation is typically only $\sim 10^{-5}$.²⁴ Even with substantial separation of 355 nm radiation in the photionization region, the majority of photons present could still be those at 355 nm.

As described under Materials and Methods (Section 2.1), 355 nm pulses in the absence of 118 nm generation (no rare gas in tripling cell) typically produced an m/z 12 peak, closely

matching the intensity of this peak with rare gas in the cell. There were also some weaker peaks at $m/z < 50$, now with minor intensity compared their detection with 118 nm generation. No other peaks were evident. The m/z 12 peak speaks to some, albeit apparently relatively minor, 355 nm multiphoton ionization accompanied by ion fragmentation.

It is also possible that residual 355 nm caused some fragmentation of parent ions produced by 118 nm PI; this phenomenon would explain the observed difference between PI-TOFMS and APCI-HR-TOFMS results. Though the experimental arrangements evidently did not allow for the observation of larger size initial cracking products, these circumstances actually offered an enhanced opportunity to observe certain more stable products of association reactions by clearing out the middle MW range. In particular, only PAHs and their fragmentation resistant precursors (presumably cyclic) were observed in 266 nm PI MB-TOFMS (Fig. 3 A'-C'), enabling the study of their link with low MW product formation. The second group of products targeted in this work, low MW products, could not be observed in earlier batch reactor studies by mass spectrometric methods for the liquid phase due to the necessity of a solvent delay to prevent the MS detector from being overwhelmed.

Residual 355 nm may account for the occasional observation of non-negligible peaks at m/z 12, 24, and even 36, C^+ , C_2^+ , and C_3^+ , respectively. Presumably these species originated from ionic fragmentation of PAH deposits formed in either the same or previous runs. Removal of one or two carbon atoms stoichiometrically results in a smaller size PAH.

3.3 Initial pyrolysis product chemistry trends (~280 °C, Figure 2, Figure S3)

3.3.1 118 nm PI: general product mass spectra

A distinctive feature in this temperature range is the appearance of several lower MW non-aromatic peaks. In most of the runs (Fig. 2, A-C, Fig. S3), a C_2 size hydrocarbon peak (ethane, 30 m/z) appears first, followed sometimes by 58 m/z (a C_4 species, likely butane, from Table 1). With further temperature rise, the diminution of these peaks appears to correlate with the rise of a broader peak, appearing in all runs, at m/z 80-86, sometimes more narrowly centered at m/z 84 (Fig. 2 A-C, Fig. S3). This peak arises from multiple C_6 species with varying degrees of unsaturation. For example, m/z 84 corresponds to hexene (Table 1). Although contributing

species could be unsaturated C₄ carboxylic acids, this alternative is less likely since the saturated member of the series, at 88 amu, was not detected.

A critical hydrocarbon product size distribution strongly correlates with a ramp-up of associative chemistry, as exemplified in Fig. 2 featuring peaks of $m/z > 200$, with more examples provided in Figs. S2 and S3. The appearance of stable C₆ products (m/z 80-86) seems to be the invariable prelude to increased associative chemistry. In effect, the stable (non-radical) C₆ products are “marker species” linked to this ramp-up.

A subsequently appearing C₇ marker species marks an even greater ramp-up of higher mass associative chemistry product peaks (see Fig. 2 A/B and Fig. S2). The enhanced production of small radical fragments is consistent with C-C bond cleavage occurring at the periphery of the fatty acid chains, with the bonds located deeper inside the carbon chain becoming accessible only under harsher conditions, *i.e.*, higher temperature.

The observed trends connecting low and high MW peak occurrence are summarized in Table 2. Both the C₆ and C₇ markers signify the facilitated occurrence of associative chemical reactions; the latter also marks the shift to three selectively formed product peaks, 276, 352 and 444 m/z , as will be shown in the subsequent sections.

When one looks at a set of successive temperature TOFMS, either for 118 nm PI or 266 nm PI, it is possible, albeit only generally, to discern correlated peak growth trends (see Fig. S2 for the pure He data series from which the mass spectra in Figs. 2 B/B' and 3 B/B' were computed). In the 118 nm PI case the C₇ marker peak gets larger as the C₆ peak decreases; similarly, the three selectively formed PAH peaks can be seen to grow relatively at higher temperatures in the 266 nm PI case. Principal component analysis can help to display such correlated product peak growth trends. For both 118 nm PI and 266 nm PI, the most important principal component, PC-1, accounts for around 70% of total variance and is a strong contributor to TOFMS at high temperatures. In the x loading plot of Fig. 4A, 118 nm PI case, growth of the C₇ marker peak is correlated with C₆ peak diminution; the C₇ marker seems to be the one most directly related to growth of higher mass species. In Fig. 4B, 266 nm PI case, the three selectively formed PAHs grow at the expense of all the non-selectively formed PAHs.

Table 2. Qualitative observations on low and high MW peak appearance in MB-TOFMS spectra.

Major low MW species	Apparent direct relationship to high MW species (including and focusing on PAHs)
C ₂ -C ₃	None
C ₄	Little or none
C ₆	Simultaneous appearance with species up to 300 amu; well developed PAH homology series
C ₇	Similar to C ₆ up to 300 amu at lower temperatures; correlation with the appearance of higher MW PAHs, up to 500 amu, at higher temperatures; eventual survival of selectively formed PAH peaks only, replacing homology series

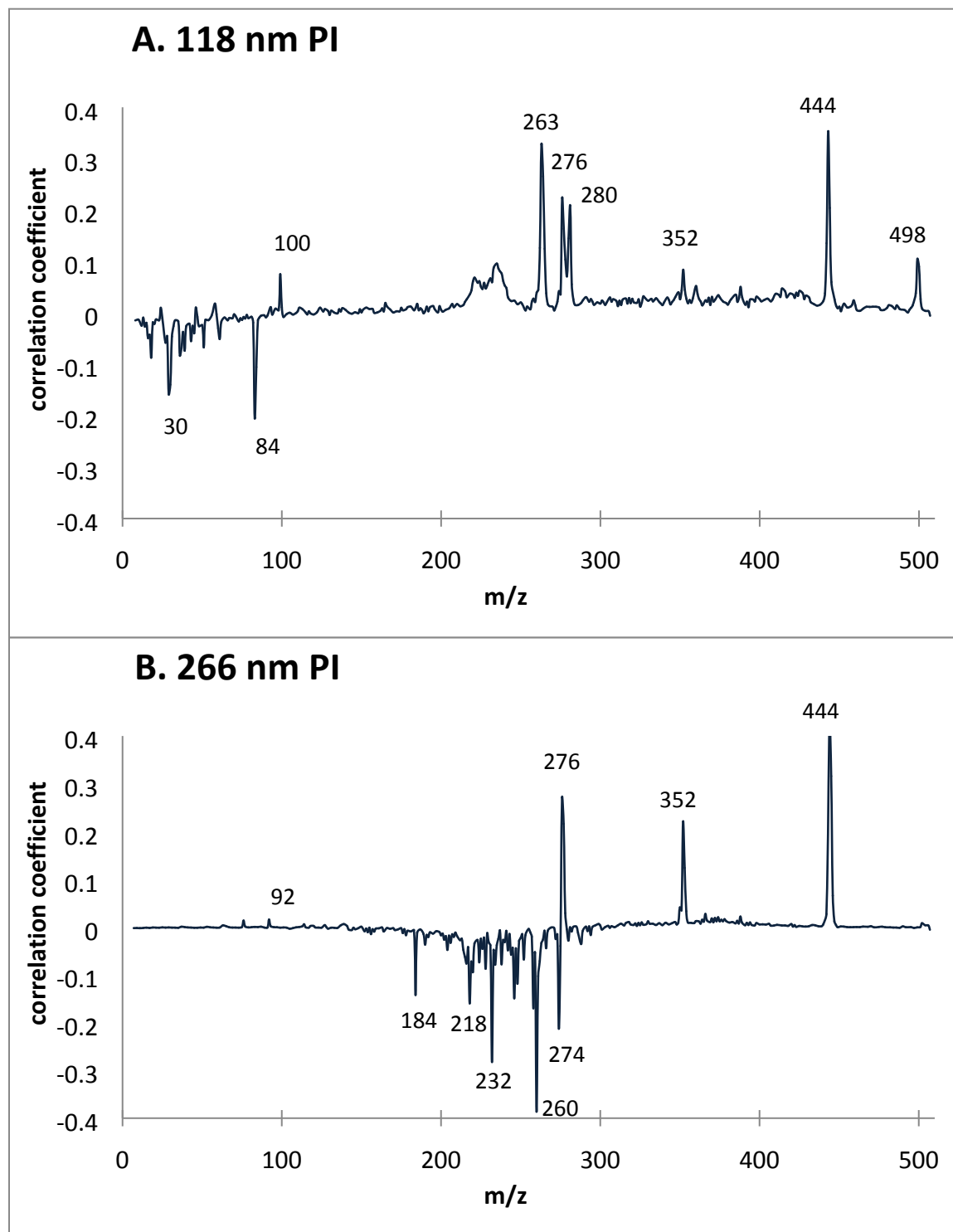


Figure 4. Computed x loadings (see text) for PC-1, the most important principal component, computed from the Figures 1-2 B series (pure He) of TOFMS for (A) 118 nm PI and (B) 266 nm PI. The y axes show relative correlated contributions.

3.3.2 118 nm PI: Influence of hydrogen

As seen in Fig. 2, there are A/B differences in this low temperature range that arguably are partly or substantially due to hydrogen gas addition. In Fig. 2A (added H₂), little or no higher MW products are present. (The fact that higher mass peaks are evident in the aromatic, 266 nm PI, mass spectrum, Fig. 2A', means that the overall aromatic product fraction must be very low.) Instead there is a different distribution of lower mass hydrocarbon products. The prominent C₇ 100 *m/z* peak has barely appeared and the trends seen in Fig. 2B (no added H₂) are more retarded. Important low mass products in the presence of hydrogen (Fig. 2A) include unsaturated C₂H₄ (28 amu) and C₃H₄ (40 amu), whereas in Fig. 2B a saturated C₂H₆ (30 amu) product has the largest prevalence. Thus, surprisingly, hydrogen addition does not necessarily lead to the predominance of double bond saturation reactions – but instead promotes general cracking reactions.

The addition of hydrogen apparently induces a smaller size product distribution at lower temperatures, with reduced growth of C₆ (*m/z* 82/86) and then C₇ (*m/z* 100) products (compare Figs. 2A and B). These results are consistent with hydrogen gas promoting early C-C bond scission to make smaller size products but with a relative hindrance to the formation of larger-size species. The foregoing observations are in accord with an earlier report that hydrogen promotes TG pyrolysis at lower temperatures.¹ These effects would be facilitated by the production of *atomic* hydrogen from the added H₂. Perhaps the glass wool that filled the sample holder aids in catalyzing pertinent gas phase reactions, particularly high energy H-H bond scission. Atomic hydrogen should also be produced *in situ* via numerous dehydrogenation reactions such as aromatization. Thus, the difference between A, B and C is quantitative rather than qualitative, *i.e.*, both A and C catch up with B at higher temperatures.

The MCR mass spectrum in Fig. 2C (118 nm PI, pure He carrier gas but different sample holder) shows pronounced differences from B as well as A. They arise mainly from much more extensive associative chemistry, leading to a considerably greater abundance of higher mass species (~100-360 *m/z*). Some of the associative chemistry products are aromatic (compare with C', the corresponding aromatic-specific mass spectra considered in the next section). Mass spectrum C also shows extensive 2 *m/z* peak structure, indicating that original fragmentation products are evolving further due to hydrogenation/dehydrogenation. A product at 98 *m/z* has

also become significant, indicating the formation of an unsaturated C_7 hydrocarbon, in contrast to A and B. Enhanced associative chemistry may arise both from enhanced medium surface area promoting it along with enhanced cracking due to the presence of hydrogen. Evidence for enhanced hydrogen occurrence in case C/C' is discussed in the next section.

3.3.3 266 nm PI: aromatic product mass spectra

The occurrence of higher mass peaks of aromatic products appears to be correlated first with the emergence of C_6 non-aromatic hydrocarbon products, then by growth of the heptane (C_7 , 100 m/z) peak (Table 2, Figs. 2 A/B and S3). This progress is suppressed by the addition of H_2 (Fig. 2A), perhaps because hydrogen quenches relevant free radicals before they can participate in associative chemical reactions. Hydrogen effects on aromatic products can be seen in Fig. 2 A'/B'. The progress toward formation of higher MW selectively formed PAHs has been inhibited in favor of lower MW aromatics, the distribution of lower mass aromatic peaks being enhanced in A'.

Both hydrogen gas (A' vs. B') and denser glass wool packing (C' vs. B') promote similar changes, in this case the survival of certain PAH precursors. In Fig. 2A', several discrete product peaks are particularly enhanced compared to 2B', m/z 184, 258/260, 274. Enhancement can also be seen at m/z 218. Trends in Fig. 2C' are somewhat analogous. There is weak appearance of m/z 184 and 218 and substantial enhancement of m/z 232, 246, 258, and 274. The m/z 232, 246, 258/260 and 274 species constitute a homology series consisting of alkyl-substituted pyrenes (*e.g.*, 258 amu) and dihydropyrenes (*e.g.*, 260 amu) or their isomers, C_{18} - C_{21} in size. The preferred and abundant formation of these specific members of this homology series can be interpreted as a combinatorial association of C_6 and C_7 size fragments ($C_6 + C_6 + C_6$, $C_6 + C_6 + C_7$, $C_6 + C_7 + C_7$ and $C_7 + C_7 + C_7$, respectively). The m/z 184 peak will be discussed subsequently.

Corroborating the trend of enhanced formation of lower MW aromatics, added hydrogen gas has promoted the appearance of a new homology series in A', appearing as clusters of peaks. This effect can be understood to arise from enhanced cracking caused by the presence of hydrogen. In our previous paper,¹² we reported similar, though relatively weaker, peak cluster series (different sample holder than A' or C'). There, however, these peaks were shifted to

higher masses by 2-4 m/z ; they therefore were assigned to homologous naphthalenes and indenenes, respectively. Now, in the presence of hydrogen, the peaks are at lower masses, m/z 126, 140 and 154. According to the stoichiometric analysis, these highly unsaturated aromatic hydrocarbons cannot be bicyclic, thus are assigned as alkadiynyl benzenes, with triple bonds in the side chains. We attribute the further unsaturation of the aromatic species in C' to dehydrogenation facilitated by a more extensive glass medium in this case.

Two lower MW species stand out, toluene (92 m/z) and one corresponding to a prominent 184 m/z peak; the latter may be either a C₄-substituted naphthalene or C₅-substituted indene dehydrogenated at the side chain, a C₁₄ species. Their significance for high MW PAH formation is discussed in subsequent sections. Without added hydrogen, these low MW peaks are barely evident.

Based on the discussion to this point, the effect of hydrogen appears to be dual: (1) enhanced presence of lower mass aromatics due to enhanced cracking and (2) damping of the growth of the higher mass selectively formed PAHs due to extensive hydrogenation. Both reactions would require atomic hydrogen generation, presumably catalyzed by glass wool.

Consistent with these conclusions, the evolution to a small number of higher MW selectively formed PAHs (276, 352 and 444 amu) is clearly more advanced in B'. Some of the significant aromatic products in C', such as m/z 258 and 274, are typically more prevalent at the *earlier* stages of PAH product chemistry. In these respects, there is more of a resemblance to A' (added hydrogen). In essence, the apparent presence of significant amounts of *in situ* produced hydrogen in C' seems to cause a proportionately massive formation of lower MW aromatics.

The observed C' to A' correlation seems to be explained by the relatively enhanced presence in each case (compared to B') of atomic hydrogen, which could be related to sheer H₂ abundance in A' or greater glass wool content in C'. As noted, hydrogen appears on the one hand to initiate association by inducing more initial radicals. On the other hand, it limits the probability of multi-step association by "quenching" the growing radicals, thereby forming either smaller MW PAHs or their immediate hydrogenated precursors.

3.4 Subsequent pyrolysis product chemistry trends (~380 °C and higher, Figure 3)

3.4.1 118 nm PI: general product mass spectra

Overall product chemistry distributions are more similar in each case at higher reaction temperatures (Fig. 3 A-C). In each instance a 100 m/z peak of similar relative intensity is present, either along with a broad 80-86 m/z peak or gradually replacing it. Concurrent with the appearance of the 100 m/z marker (heptane, C_7), significant higher MW peaks are evident, indicating enhanced association reactions (Table 2). Fig. 3 panels A, B, and C all display fairly similar relative ratios of 263 and 280 m/z non-aromatic products, with similar 276 m/z aromatic product peaks as well. However, compared to B (He only), mass spectrum A (H_2 added) shows an additional non-aromatic product at 270 amu. It could be a non-aromatic analog of the observed abundant PAHs with 258 and 260 m/z .

Developments at higher temperature appear to mark the onset of significant TG cracking that produces ample hydrogen, also coupled with the largescale onset of associative chemical reactions. The onset temperature for significant TG pyrolysis in the MB study appears to match the one observed in the bulk product analysis study.¹

3.4.2 266 nm vs.118 nm PI: mass spectra of the most abundant PAHs and their non-aromatic precursors

The selectively formed aromatic peaks become more pronounced as the temperature increases (primed letter peaks in Fig. 3 versus Fig. 2, peak correlations/anticorrelations in Fig. 4B). The disproportionate growth of these products is consistent with the observation that the abundant formation of C_6 and then C_7 reactive fragments triggers PAH formation. The main such PAH peaks are at 276, 352 and 444 m/z (Fig. 3 A'-C'). In these cases there may be corresponding "satellite" non-aromatic peaks appearing in the 118 nm PI spectra at MW values slightly higher than the corresponding aromatic peaks (Fig. 3 A-C). For example, next to the 352 m/z peak, there is also a weak non-aromatic mass peak at 360 m/z . Based on observations of its subsequent growth pattern in many experiments, it arises from association of several smaller fragments resulting from oleic acid pyrolysis, as previously discussed.¹² These satellites may be eventual PAH precursors that require additional dehydrogenation for aromatization. Such intermediates are most likely cyclic, explaining their relative survival from fragmentation characteristic of other non-aromatic products.

In the 118 nm PI-TOFMS (Fig. 3 A-C), all peak heights are in rough proportion to relative species concentrations. As we reported earlier for 118 nm PI-TOFMS, the ratio of these

PAH peaks to non-aromatic species peaks was significantly smaller with glass beads than with glass wool.¹¹ These combined observations point to significantly greater facilitation of dehydrogenation reactions on the surface of glass wool, presumably due to its high surface area. The C vs. B effects—both glass wool media—are less pronounced than glass beads vs. glass wool media.

3.4.3 266 nm PI: trends in aromatic product mass spectra

A clearer and more conspicuous difference arises between C' vs. B' in these spectra (see Fig. 2), evidently due to a denser glass wool medium. B' shows a growing predominance of m/z 352, then overtaken by m/z 444.¹² These trends are significantly less developed in C'. There are some correlated trends in the 118 nm PI. The aromatic m/z 444 peak is markedly absent in C; so is the non-aromatic m/z 498 peak. The absence of m/z 498 indicates that the fragment number densities needed for its formation must be much lower in C; the same also must hold for m/z 444. As stated throughout this paper, this difference may be due to abundant *in situ* formation of reactive atomic hydrogen in C, which quenches the radical producing/growing sites more effectively than molecular hydrogen in A/A'. As a result, there are only 2-3 fragment associations rather than 4-5.

Notably, long homology profiles observed at lower temperatures disappear in this higher temperature regime, now replaced by single hydrocarbons of distinct sizes (Table 2, Fig. 4). These outcomes point to specific combinations of fragments of certain sizes as well as the survival of only select species, presumably the most stable PAHs (likely fully conjugated and non-substituted). Unlike the wider range of aromatics at lower temperatures, the stoichiometrically determined numbers of carbon atoms in these PAHs (C_{22} , C_{28} and C_{36} for 276, 352 and 444 amu, respectively) are correlated with the most likely sized “building blocks,” 7 or 8 carbon atoms rather than 6.

Multivariate principal component analysis applied to the aromatic product case (266 nm PI), Fig. 4B, shows that the selectively formed PAHs (photoions at m/z 276, 352, 444) grow at the expense of all the non-selective lower-MW PAHs. For numerous separate sequences of experimental runs, reflecting slightly different sample handling conditions, the PC-1 x loadings computed from the 266 nm PI series of TOFMS consistently show a positive peak at m/z 92,

toluene, often more prominent than in Fig. 4B and usually with no other lower mass peaks. Toluene, the C₇ aromatic hydrocarbon, would arise from “quenched” benzyl radicals that did not participate in the further growth of the selectively formed PAHs, as discussed further throughout the paper. Similarly, as mentioned in the section on low-temperature aromatic products, the peak at 184 *m/z*, attributed to a C₁₄ aromatic species, becomes most abundant in the presence of hydrogen, indicating that this is another quenched intermediate of high-MW PAH formation. It is notable that the C₇ and C₁₄ aromatic peaks are, by far, most prominent within the corresponding homology series, thus emphasizing their significance. The significance of C₇ sized intermediates was verified in batch reactor studies reported in the next section.

3.5 Batch reactor results

3.5.1 Homology patterns of canola oil pyrolysis products obtained in a batch reactor

The liquid phase products account for 55-60 w/w% of the original feedstock (canola oil); an additional 10-25% became coke and tar and the rest gaseous products.^{1,3} When all GC-recovered products are added up, including the estimates for unresolved and unidentified compounds,¹⁰ mass balance closes to 90-95% within the liquid phase (not shown). This indicates that the concentration of high MW non-GC elutable products is insignificant.

The homology profiles of all products, all hydrocarbon products (*i.e.*, without carboxylic acids) and *n*-alkanes are shown in Fig. 5, panels A-C, respectively. According to these data, canola oil thermal cracking products are rich in C₆-C₉ species. The homology pattern is consistent with a predominant C-C bond break occurring at the allylic position to the ω-9 double bonds. This pattern, in turn, is consistent with the observed abundance of C₆-C₇ species peaks in MB-TOFMS and their proposed role as markers of pronounced TG cracking.

The observed predominance of C₅-C₉ hydrocarbons in batch reactor experiments and relative absence of the complementary peak of occurrence, at C₁₁ (Fig. 2C), is consistent with the allylic C-C bond scission occurring preferentially on the ω-side of the ω-9 double bond. This double bond is present in all major naturally occurring unsaturated fatty acids. Apparently, long chain alkenyl radicals formed upon the non-symmetric scission of the original C₁₈ fatty acid on the α-side (C₁₁ and longer) are not converted to *n*-alkanes, instead yielding other hydrocarbon products. This conclusion is supported in Fig. 5C, pertaining only to alkanes. Note the

discontinuous drop-off in the distribution in going from C_9 to C_{10} . On the other hand, Fig. 5B, which accounts for all the hydrocarbons, is a smoother distribution than Fig. 5C. In conclusion, longer fragments end up becoming other, unsaturated/cyclic hydrocarbons recovered in the liquid phase (their analysis was published earlier³). Fig. 5A shows a still more even profile for all products. This is because C_2 and C_3 carboxylic acids are much less volatile than the corresponding alkanes, so their recovery by GC is significantly more complete.

A relatively high abundance of the C_{15} and C_{17} linear alkanes (Fig. 5A) is apparently due to the alkyl radicals formed from the original TG FAs via decarboxylation. Alkanes are relatively abundant only up to and including C_{17} . A sizable drop in abundance is observed for higher homologues (Fig. 5C). Note that the C_{17} hydrocarbon is the largest one that may be directly formed from C_{18} fatty acid chains contained in TGs. Higher MW alkanes ($>C_{17}$) must be formed via radical recombination (doubling), which would explain their much smaller amounts. This trend is even more pronounced for the homology profiles of total hydrocarbons. (See how abruptly the pattern ends at C_{17} in Fig. 5B.) The foregoing observations indicate that the gas phase pyrolytic reactions (ultimately yielding liquid phase products in batch reactors) lack virtually any degree of fragment condensation, in stark contrast to the solid phase reactions leading to coke formation.

Furthermore, the PAHs recovered in the liquid phase were only bicyclic (indanes and naphthalenes), $<C_{17}$ size,³ in contrast to the large size PAHs observed in the MB work. These observations are consistent with the previously stated assumption that larger PAHs are coke precursors, therefore not appearing among the liquid phase TG cracking products.¹²

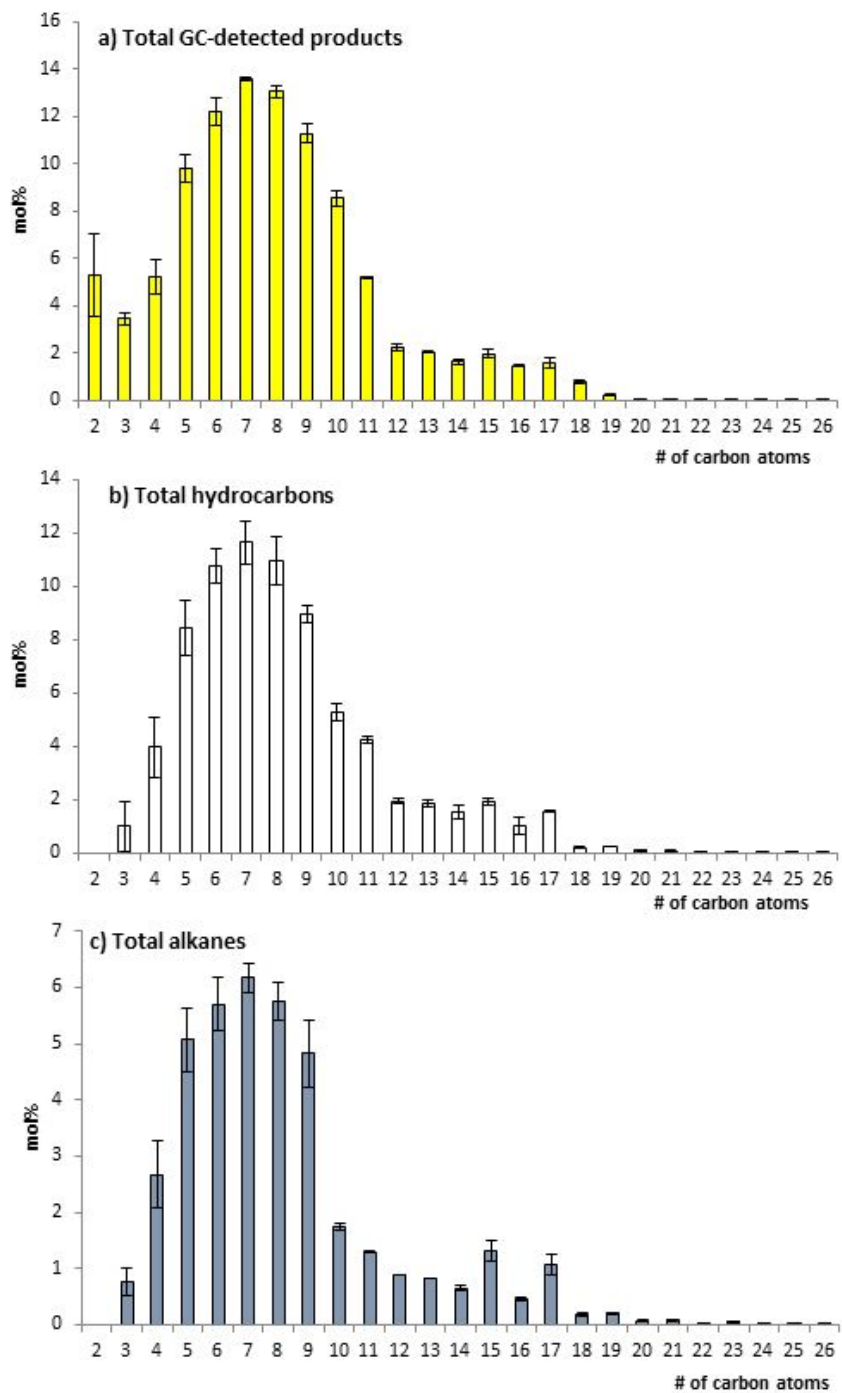


Figure 5. Homology profiles of hydrocarbon liquid phase products of canola oil pyrolysis

3.5.2 Connection between the MB-TOFMS and batch reactor studies

High MW PAHs (276, 352 and 444 amu) are characteristic for MB-TOFMS but are absent in batch reactor liquid phase products. Obviously, the observation of these gas phase species as they exit the pinhole in MB experiments means that sufficient association chemistry has occurred to produce them. In contrast, the association chemistry occurring in ~ 1 h in batch reactors leads to different terminal outcomes. While similar PAHs may have appeared initially, they continue undergoing association to result in coke and tars. Corroborating observations were recently made by Fanglin et al., who extracted high MW PAHs from tars formed as a result of TG pyrolysis, while such PAHs were not recovered among the liquid phase products.¹⁸ The generated solid phase may serve as a catalyst for numerous heterogeneous reactions (similar to glass wool in MB-TOFMS experiments), including C-H bond scission, resulting in atomic hydrogen formation.

The batch reactor hydrocarbon product homology profiles, though broader than those obtained by MB-TOFMS, match the predominant C_7 size of primary decomposition products. The predominance of C_7 size fragments, as opposed to the kinetically controlled generation of smaller fragments, can be explained by the thermodynamically favored C-C bond cleavage at the allylic position to the $\omega-9$ double bond. The appearance of a strong 100 m/z peak at higher temperatures appears to signify a switch to thermodynamic factors, *i.e.*, when all C-C bonds become accessible. Once the switch occurs, larger fragments than C_7 , C_8 - C_{10} , are less likely to form as a result of primary cracking reactions, due to much larger bond energies when the cleavage occurs closer to or at the double bond.² The MB-TOFMS experiments show that high MW species start forming in abundance at this point as a result of fragment condensation reactions—but only in the segregated solid phase contacting the gas phase (as opposed to the bulk liquid phase), leading to higher-MW PAH formation. The relatively broad homology profile in the batch reactor is presumably due to much longer reaction times, randomizing the C-C bond scission pattern.

While both saturated and unsaturated/cyclic hydrocarbons occur without any preference for C_6 or C_7 among the liquid phase products (Figs. 5B and C), the MB-TOFMS product profile shows the prevalent (virtually, exclusive) occurrence of the saturated C_7 product (heptane, 100 amu) rather than C_6 hydrocarbons varying in their unsaturation extent (82-86 amu, Fig. S3). It

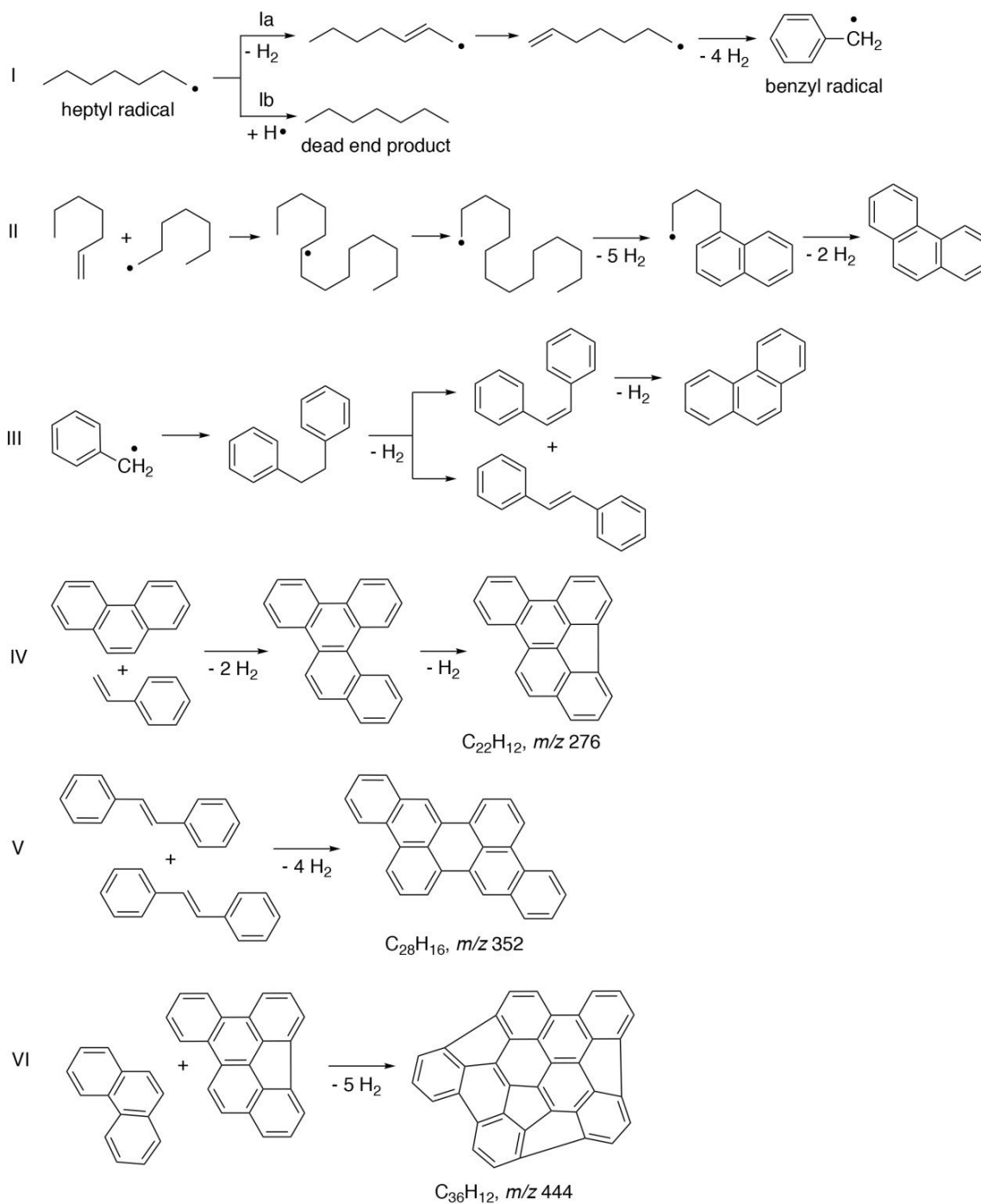
may be that unsaturated C_7 size intermediates also form in abundance in MB-TOFMS experiments, but then are immediately consumed in association reactions. In our previous publication,¹² we provided arguments (based on both literature and our experiments) that C_7 -sized alkenyl radicals are more reactive in association reactions than their C_6 analogs because they lead to the formation of benzyl radicals, which are relatively stable yet trigger further association. The observed formation of toluene (Figs. 2-4, see panels A'-C' in Figs. 2 and 3), presumably as a result of quenching of benzyl radicals with hydrogen, is consistent with this suggestion.

It is notable that batch reactor thermal TG cracking is conducted under significant pressure, >200 atm.¹⁻³ Under ambient pressure, a yellow solid (apparently cross-linked) polymer is formed instead that decomposes only at very high temperatures to yield coke and gases, with virtually no liquid products. This observation may explain the observed difference between the MB-TOFMS and batch reactor liquid phase TG pyrolysis products. Under high pressure the reaction occurs in the liquid (or pseudo-liquid, subcritical) phase, where conditions may reduce the probability of intermolecular chemical reactions occurring within or on the surface of the solid phase.

3.6 Plausible pathways for high MW PAH formation

This section will be focused on the formation of the most abundant PAHs corresponding to the 276, 352 and 444 m/z peaks, $C_{22}H_{12}$, $C_{28}H_{16}$ and $C_{36}H_{12}$, respectively. They account for a surprisingly large fraction of the observed PAH products, suggesting significant selectivity in their formation. Based on previous arguments,¹² we narrowed the list of key candidate precursor intermediates from C_7 - C_{11} to just C_7 in size. Fully conjugated PAHs with $7 \times 2 = 14$ (anthracene or phenanthrene) and $7 \times 4 = 28$ carbon atoms are known and common. By contrast, fully conjugated PAHs with $7 \times 3 = 21$ and $7 \times 5 = 35$ carbon atoms do not exist, thus necessitating the replacement of one of the C_7 fragments with C_8 . This conclusion is consistent with the C_{22} and C_{36} PAHs actually observed. The increasing predominance of the C_{28} and C_{36} PAH products in the TOFMS is consistent with the stability of non-substituted fully conjugated PAHs. Formation of such products is also observed in flames.¹⁶ Possible pathways of formation of all

three abundantly occurring PAHs are shown in Scheme 2, using the assumption of fully conjugated non-substituted PAHs. We will discuss their potential precursors. We will not



Scheme 2. Possible paths and reactions of PAH formation.

consider the less abundant PAHs formed via condensation of fragments of other size; they occur non-selectively at lower temperatures, as discussed in the previous sections.

We identified toluene 92 m/z , as a notable peak, since it can be viewed as a marker, a quenched version, of the benzyl radical. The arguments of the preceding paragraph indicate the need for associative chemistry also involving C_8 species. In this context, an observed 104 m/z peak, styrene (see Fig. 2A'), appears to be a marker for C_8 association chemistry species. The fact that this peak is smaller than the C_7 marker is because there are more reactive C_7 intermediates present than reactive C_8 . By contrast, in Fig. 2B' the styrene peak has disappeared and the toluene peak is now barely discernible. As indicated throughout this paper, additional hydrogen has deactivated more of the reactive species, resulting in larger C_7 and C_8 peaks (Fig. 2A'). We pointed out that the appearance of C_6 sized compound peaks marked a prelude to significant associative chemistry, that they may be directly involved in the intermediate PAH formation at relatively low temperatures. However, unlike C_8 , C_6 reactive species do not appear to be involved directly in the *high-temperature* associative chemistry leading to the selectively formed PAH products (Table 2).

Based on the C_7 size, a heptyl radical appears to be the key intermediate starting the chain of reactions leading to PAH structures (reaction I, Scheme 2). If atomic hydrogen is abundant, heptane is formed as a dead-end product in the competing path (reaction Ib). Alternatively, radical stabilization via dehydrogenation can lead to a heptenyl radical, starting the sequence that leads to PAH formation. Since no heptene was observed among products in the 118 nm PI-TOFMS, this postulated intermediate appears to proceed substantially to formation of benzyl radicals (reaction Ia). The stable hydrogenated marker species form of benzyl radical, toluene ($m/z=92$), is relatively abundant among the aromatic products.

Further along the indicated pathways, essential reactions of cyclization, addition and double bond migration are known to have low activation energies.²⁵⁻²⁹ One of the potential paths (II), involving radical addition to 1-heptene, ultimately yields a C_4 -substituted naphthalene, with a subsequent formation of phenanthrene. An alternate path could be the isomerization of 1-butyl naphthalene (or its radical) to slightly more stable 2-butyl naphthalene, with the ultimate formation of anthracene instead of phenanthrene. As we have noted, C_{14} -sized hydrocarbons, particularly a prominent 184 m/z peak, were observed in low temperature MB-TOFMS

experiments at intermediate temperatures as the most abundant members of the corresponding homology series (Figs. 2, 4B).

By contrast, dehydrogenation reactions may be unlikely unless facilitated by the formation of highly conjugated π bond networks. They also have lower activation energies when occurring in the condensed phase.³⁰ The observation of highly dehydrogenated intermediate products at lower temperatures indicates that these reactions are not prohibited in MB experiments. At higher temperatures, the direct observation of PAHs and their non-aromatic “satellites” in 118 nm PI spectra are consistent with this conclusion (Figs. 2 and 3). As pointed out throughout this paper, these reactions appear to be facilitated by the glass wool surface.

One facilitated dehydrogenation reaction well known in synthetic chemistry is shown in Scheme 2 as reaction III. Doubling of benzyl (and also indenyl) radicals is considered as one of the main paths of PAH formation in combustion reactions.^{31,32} In those instances stilbene is converted to phenanthrene with a very low activation energy, 13 kJ/mol.³² This reaction is also used in synthetic chemistry to produce large PAHs.³³ The peaks of both phenanthrene ($m/z=178$) and its precursor, stilbene ($m/z=180$), along with their more hydrogenated precursor ($m/z=184$), are observed among the products at intermediate temperatures (Figs. 2 A'-C' and 4B). However, an alternate pathway bypassing stilbene, through dihydrophenanthrene formation, was observed under combustion conditions.¹⁵

We cannot definitively state which of the two reactions, II or III, is more plausible. On the one hand, reaction II assumes a rather fortuitous series of cyclizations. On the other hand, reaction III assumes a significant abundance of benzyl radicals. Multiple in-between cases are also possible: benzyl radicals may attack either double bonds or aromatic intermediates to yield larger aromatic structures.

Once either phenanthrene or its partially hydrogenated C_{14} precursors are formed, they are less likely to react with another C_7 fragment, since none of the unsubstituted C_{21} PAHs ($C_{21}H_{12}$) is fully conjugated (as in the case of indane, C_9H_8). By contrast, the C_{22} ($C_{22}H_{12}$) PAHs ($m/z=276$) are conjugated; one such isomer is shown in reaction IV. Even though a direct high temperature styrene reaction with phenanthrene has not been reported, styrene is well known to undergo thermal dimerization,³⁴ Diels-Alder addition,³⁵ polymerization³⁶ or co-polymerization.³⁷ Thus this reaction is plausible, given that it forms a highly conjugated product with the release of three H_2 molecules. An alternate path may involve the reactions of the corresponding free

radicals: inter-PAH reactions are known to be facilitated by the addition of free radical sources.³⁸

The doubling of C₁₄ precursors of phenanthrene (*e.g.*, *trans*-stilbene) may lead to a C₂₈ PAH (C₂₈H₁₆, *m/z*=352, reaction V). In this case, intermolecular dehydrogenation would be facilitated by significant additional aromatization. An alternate path is the attachment of two separate C₇ fragments, one by one, to either stilbene or phenanthrene or their C₁₄ precursors.

Finally, the C₃₆ PAH (C₃₆H₁₂, *m/z* 444) is likely formed from the C₂₂ PAH as a result of reaction with *cis*-stilbene (reaction VI) or phenanthrene/precursors, or by two consecutive reactions with C₇ fragments. It may also be formed by the reaction of a C₂₈ PAH (or its hydrogenated precursors) with styrene. Note that a C₃₆H₁₀ hydrocarbon cannot occur as a common planar PAH molecule since more hydrogens would have to occupy the pertinent positions on its periphery. Elimination of those extra hydrogens is possible only when dome-like structures, characteristic of fullerene precursors, are formed,³⁹ as illustrated in Scheme 2 by the distortions in the structure of the product of reaction VI.

The ultimate formation of fullerene (*i.e.*, soot) precursors at high temperatures is expected. We previously reported that at high temperatures all low MW PAHs proceed to vanish at the expense of the one with *m/z* 444.¹² Based on the prevalence of C₇ fragments and stoichiometric considerations applied in this work, this phenomenon may result from a direct conversion of smaller PAH precursors while adding C₇ (and C₈ whenever necessary) fragments.

Conclusions

Significant pyrolytic chemical reactions in the MB experiments were first observed below 300 °C. They commence with decomposition reactions yielding small fragments (C₁-C₄ in size, growing with temperature), eventually marked by the appearance of a ~84 *m/z* peak. It is in this relatively low temperature regime that H₂ addition has its clearest effect. The result is an enhancement of lower mass (< ~100 amu) overall products, with the appearance of a new MS marker species for associative chemistry at 100 *m/z*. This marker product, heptane, also appears in the runs with the He carrier gas, but at higher temperatures. Its facile production is expected to occur by the C-C bond cleavage at the allylic position to the oleic acid double bond (Scheme 1), thus being consistent with organic chemistry based mechanistic considerations. The formation

of C₆-C₇ markers appears related to enhanced association chemical reactions leading to PAH precursors; higher MW products are seen to form at high temperatures when the C₇ marker becomes prevalent. For the subset of products that are aromatic, the effect of hydrogen is an enhancement of aromatics of lower mass. A different MB sample preparation resulted in significant shift of all products, particularly, aromatic, toward lower MW, apparently related to hindering of intermolecular, associative reactions as a result of enhanced *in situ* atomic hydrogen formation. PAHs formed in the MB experiments were shown to undergo reactions with C₇ and C₈ aromatic fragments leading to formation of higher MW PAH products. The PAHs observed at high temperatures appear to result from the association of 3-5 such fragments, ultimately forming soot precursors. By contrast, the association reactions at lower temperatures leading to homology series of substituted PAHs appear to include C₆ fragments as well.

Conflicts of interest

There are no conflicts of interest.

Acknowledgements

MS gratefully acknowledges support from the Tulane Committee on Research, the Carol Lavin Bernick Faculty Grant Program, and the Army Research Office grant 555955G1. Funding for WS, AK, EK and their students was provided by the U.S. Department of Energy, the North Dakota Agricultural Production Utilization Commission, the North Dakota State Board of Agricultural Research, the North Dakota Soybean Council, and the National Science Foundation (e.g., NSF ND EPSCoR Track I CSMS IIA-1355466 2014-19 award). Neither the United States Government nor any agency thereof, nor any of their employees, makes any warranty, express or implied, or assumes any legal liability or responsibility for the accuracy, completeness, or usefulness of any information disclosed. Reference herein does not necessarily constitute or imply its endorsement, recommendation, or favoring by the United States Government or any agency thereof or by the State of North Dakota.

The authors would like to acknowledge the contributions of the following individuals in this work: Ted Aulich, Ron Timpe and Jerry Petersburg of the UND Energy and Environmental Research Center; Yan Luo, A. Mojtaba Sadrameli and Joe Miller of the UND Chemical

Engineering Department; Irina Smoliakova of the UND Chemistry Department for her incisive reading and comments.

Associated Content

APCI mass spectra, additional molecular beam TOFMS, table of less expected species for possible correlation with observed low mass species in molecular beam TOFMS.

References

1. Kubatova, A.; Luo, Y.; Stavova, J.; Sadrameli, S. M.; Aulich, T.; Kozliak, E.; Seames, W. *New path in the thermal cracking of triacylglycerols (canola and soybean oil)*. *Fuel* **2011**, *90*[8], 2598-2608.
2. Kubatova, A.; Geetla, A.; Casey, J.; Linnen, M. J.; Seames, W. S.; Smoliakova, I. P.; Kozliak, E. I. *Cleavage of carboxylic acid moieties in triacylglycerides during non-catalytic pyrolysis*. *Journal of the American Oil Chemists' Society* **2015**, *92*[5], 755-767.
3. Kubátová, A.; St'avova, J.; Seames, W. S.; Luo, Y.; Sadrameli, S. M.; Linnen, M. J.; Baglayeva, G. V.; Smoliakova, I. P.; Kozliak, E. I. *Triacylglyceride Thermal Cracking: Pathways to Cyclic Hydrocarbons*. *Energy Fuels* **2012**, *26*[1], 672-685.
4. Boffito, D. C.; Galli, F.; Pirola, C.; Patience, G. S. *CaO and isopropanol transesterify and crack triglycerides to isopropyl esters and green diesel*. *Energy conversion and management* **2017**, *139*, 71-78.
5. Wang, H.; Lin, H.; Feng, P.; Han, X.; Zheng, Y. *Integration of catalytic cracking and hydrotreating technology for triglyceride deoxygenation*. *Catalysis Today* **2017**, *291*, 172-179.
6. Zhao, X.; Wei, L.; Cheng, S.; Cao, Y.; Julson, J.; Gu, Z. *Catalytic cracking of carinata oil for hydrocarbon biofuel over fresh and regenerated Zn/Na-ZSM-5*. *Applied Catalysis A: General* **2015**, *507*, 44-55.
7. Morgan, T.; Santillan-Jimenez, E.; Harman-Ware, A. E.; Ji, Y.; Grubb, D.; Crocker, M. *Catalytic deoxygenation of triglycerides to hydrocarbons over supported nickel catalysts*. *Chemical Engineering Journal* **2012**, *189*, 346-355.
8. Dupain, X.; Costa, D. J.; Schaverien, C. J.; Makkee, M.; Moulijn, J. A. *Cracking of a rapeseed vegetable oil under realistic FCC conditions*. *Appl.Catal., B* **2007**, *72*[1-2], 44-61.
9. Štávová, J.; Beránek, J.; Nelson, E. P.; Diep, B. A.; Kubátová, A. *Limits of detection for the determination of mono- and dicarboxylic acids using gas and liquid chromatographic methods coupled with mass spectrometry*. *Journal of Chromatography B* **2011**, *879*[17-18], 1429-1438.
10. Štávová, J.; Stahl, D. C.; Seames, W. S.; Kubátová, A. *Method development for the characterization of biofuel intermediate products using gas chromatography with simultaneous mass spectrometric and flame ionization detections*. *Journal of Chromatography A* **2012**, *1224*, 79-88.

11. Alhroub, I.; Shen, W.; Yan, J.; Sulkes, M. *Thermal cracking of triacylglycerols: Molecular beam studies*. Journal of Analytical and Applied Pyrolysis **2015**, *115*, 24-36.
12. Alhroub, I.; Kozliak, E.; Kubatova, A.; Sulkes, M. *PAH/Aromatic Tar and Coke Precursor Formation in the Early Stages of Triglyceride (Triolein) Pyrolysis*. The Journal of Physical Chemistry A **2018**, *122* (12), 3238-3249.
13. Zhao, L.; Prendergast, M.; Kaiser, R. I.; Xu, B.; Ablikim, U.; Lu, W.; Ahmed, M.; Oleinikov, A. D.; Azyazov, V. N.; Howlader, A. H. *How to Add a Five-Membered Ring to Polycyclic Aromatic Hydrocarbons (PAHs) - Molecular Mass Growth of the 2-Naphthyl Radical (C₁₀H₇) to Benzindenes (C₁₃H₁₀) as a Case Study*. Physical Chemistry Chemical Physics **2019**.
14. NIST Polycyclic Aromatic Hydrocarbon Structure Index <http://pah.nist.gov/>.
15. Hirsch, F.; Constantinidis, P.; Fischer, I.; Bakels, S.; Rijs, A. M. *Dimerization of the Benzyl Radical in a High-Temperature Pyrolysis Reactor Investigated by IR/UV Ion Dip Spectroscopy*. Chemistry - A European Journal **2018**, *24*[30], 7647-7652.
16. Mueller, L.; Jakobi, G.; Orasche, J.; Karg, E.; Sklorz, M.; Abbaszade, G. Ā.; Weggler, B.; Jing, L.; Schnelle-Kreis, J.; Zimmermann, R. *Online determination of polycyclic aromatic hydrocarbon formation from a flame soot generator*. Analytical and bioanalytical chemistry **2015**, *407*[20], 5911-5922.
17. Oektem, B.; Tolocka, M. P.; Zhao, B.; Wang, H.; Johnston, M. V. *Chemical species associated with the early stage of soot growth in a laminar premixed ethylene-oxygen-argon flame*. Combustion and Flame **2005**, *142*[4], 364-373.
18. Fanglin, L.; Liu, P.; Qiaolong, Z.; Jiang, J.; Wang, F.; Hse, C.; Xu, J. *Catalytic cracking of triglycerides with a base catalyst and modification of pyrolytic oils for production of aviation fuels*, Sustainable Energy & Fuels **2018**, *2*[6], 1206-1215.
19. Kubicka, D.; Šimáček, P.; Žilková, N. *Transformation of vegetable oils into hydrocarbons over mesoporous-alumina-supported CoMo catalysts*. Topics in Catalysis **2009**, *52* [1-2], 161-168.
20. Jenišťová, K.; Hachemi, I.; Mäki-Arvela, P.; Kumar, N.; Peurla, M.; Capek, L.; Wärnå, J.; Murzin, D. Y. *Hydrodeoxygenation of stearic acid and tall oil fatty acids over Ni-alumina catalysts: Influence of reaction parameters and kinetic modelling*. Chemical Engineering Journal **2017**, *316*, 401-409.
21. Mao, J.; Jiang, D.; Fang, Z.; Wu, X.; Ni, J.; Li, X. *Efficient hydrothermal hydrodeoxygenation of triglycerides with in situ generated hydrogen for production of diesel-like hydrocarbons*. Catalysis Communications **2017**, *90*, 47-50.

22. Shin, E. J.; Nimlos, M. R.; Evans, R. J. *A study of the mechanisms of vanillin pyrolysis by mass spectrometry and multivariate analysis*. *Fuel* **2001**, *80* (12), 1689-1696.
23. Li, J.; Wang, Y.; Wang, F.; Liang, S.; Lin, X.; Chen, X.; Zhou, J. *A study on ionization potential and electron trap of vegetable insulating oil related to streamer inception and propagation*. *Physics Letters A* **2017**, *381*[44], 3732-3738.
24. McCann, M. P.; Chen, C. H.; Payne, M. G. *Two-photon (vacuum ultraviolet+ visible) spectroscopy of argon, krypton, xenon, and molecular hydrogen*. *The Journal of chemical physics* **1988**, *89*[9], 5429-5441.
25. Raj, A.; Al Rashidi, M. J.; Chung, S. H.; Sarathy, S. M. *PAH growth initiated by propargyl addition: Mechanism development and computational kinetics*. *The Journal of Physical Chemistry A* **2014**, *118*[16], 2865-2885.
26. Bian, H.; Wang, Z.; Zhang, F.; Wang, Z.; Zhu, J. *Unimolecular Reaction Properties for the Long-Chain Alkenyl Radicals*. *International Journal of Chemical Kinetics* **2015**, *47* [11], 685-694.
27. Wang, K.; Villano, S. M.; Dean, A. M. *Reactivity-structure-based rate estimation rules for alkyl radical H atom shift and alkenyl radical cycloaddition reactions*. *The Journal of Physical Chemistry A* **2015**, *119* [28], 7205-7221.
28. Myshkin, V. E.; Shostenko, A. G.; Zagorets, P. A. *Rate constants of alkyl radical addition to olefins*. *Kinet. Katal.* **1979**, *20*[2], 298-301.
29. Degirmenci, I.; Coote, M. L. *Comparison of thiyl, alkoxy, and alkyl radical addition to double bonds: the unusual contrasting behavior of sulfur and oxygen radical chemistry*. *The Journal of Physical Chemistry A* **2016**, *120*[10], 1750-1755.
30. Indarto, A.; Giordana, A.; Ghigo, G.; Maranzana, A.; Tonachini, G. *Polycyclic aromatic hydrocarbon formation mechanism in the "particle phase". A theoretical study*. *Physical Chemistry Chemical Physics* **2010**, *12*[32], 9429-9440.
31. Sinha, S.; Rahman, R. K.; Raj, A. *On the role of resonantly stabilized radicals in polycyclic aromatic hydrocarbon (PAH) formation: pyrene and fluoranthene formation from benzyl-indenyl addition*. *Physical Chemistry Chemical Physics* **2017**, *19*[29], 19262-19278.
32. Sinha, S.; Raj, A. *Polycyclic aromatic hydrocarbon (PAH) formation from benzyl radicals: a reaction kinetics study*. *Physical Chemistry Chemical Physics* **2016**, *18*[11], 8120-8131.
33. Talele, H. R.; Chaudhary, A. R.; Patel, P. R.; Bedekar, A. V. *Expeditious synthesis of helicenes using an improved protocol of photocyclodehydrogenation of stilbenes*. *Arkivoc* **2011**, *9*, 15-37.

34. Mayo, F. R. *The dimerization of styrene*. Journal of the American Chemical Society **1968**, *90*[5], 1289-1295.
35. Pryor, W. A. *Spontaneous polymerization of vinyl monomers. Diradical and Diels-Alder mechanisms*. Polym. Prepr. , Amer. Chem. Soc. , Div. Polym. Chem. **1971**, *12*[1], 49-55.
36. Sanson, J. F. *Short-chain polymers from styrene or its homologs*. FR1229818, Sep 9, 1960.
37. Nagasako, T.; Shimada, M.; Okuyama, K. *Measurement and analysis of styrene thermal polymerization in a laminar tubular reactor*. Kagaku Kogaku Ronbunshu **1996**, *22* [4], 907-915.
38. Amick, A. W.; Martin, S. E. *Use of External Radical Sources in Flash Vacuum Pyrolysis to Facilitate Cyclodehydrogenation Reactions in Polycyclic Aromatic Hydrocarbons*. Australian Journal of Chemistry **2014**, *67*[9], 1338-1343.
39. Ansems, R. B.; Scott, L. T. *Circumtrindene: A geodesic dome of molecular dimensions. Rational synthesis of 60 of C60I*. Journal of the American Chemical Society **2000**, *122*[12], 2719-2724.

Influence of Early Stages of Triglyceride Pyrolysis on the Formation of PAHs as Coke Precursors

Evguenii Kozliak, Mark Sulkes, Ibrahim Alhroub, Alena Kubátová, Anastasia Andrianova, Wayne Seames

Molecular beam mass spectrometry has been used to investigate thermal decomposition of triolein, to reveal the mechanisms of low temperature soot formation characteristic for triglycerides (TGs).

